Journal of Solid State Chemistry 184 (2011) 1304–1311

Contents lists available at ScienceDirect

Journal of Solid State Chemistry

journal homepage: www.elsevier.com/locate/jssc

Surfactant-assisted hydrothermal crystallization of nanostructured lithium metasilicate (Li_2SiO_3) hollow spheres: (I) Synthesis, structural and microstructural characterization

J. Ortiz-Landeros [a,b], M.E. Contreras-García [c], C. Gómez-Yáñez [b], H. Pfeiffer [a,*]

[a] Instituto de Investigaciones en Materiales, Universidad Nacional Autónoma de México, Circuito exterior s/n, Ciudad Universitaria, Del. Coyoacán, CP 04510, México DF, Mexico
[b] Departamento de Ingeniería Metalúrgica, Escuela Superior de Ingeniería Química e Industrias Extractivas, IPN, UPALM, Av. Instituto Politécnico Nacional s/n, CP 07738, México DF, Mexico
[c] Instituto de Investigaciones Metalúrgicas, Universidad Michoacana de San Nicolás de Hidalgo, Francisco J. Mújica s/n Edificio U Ciudad Universitaria, CP 58060, Morelia Michoacán, Mexico

ARTICLE INFO

Article history:
Received 4 December 2010
Received in revised form
22 March 2011
Accepted 29 March 2011
Available online 6 April 2011

Keywords:
Lithium metasilicate
Hydrothermal crystallization
Chemical synthesis
Lithium silicates

ABSTRACT

Lithium metasilicate (Li_2SiO_3) was successfully synthesized using a hydrothermal process in the presence of different surfactants with cationic, non-ionic and anionic characters. The samples obtained were compared to a sample prepared by the conventional solid-state reaction method. The structural and microstructural characterizations of different Li_2SiO_3 powders were performed using various techniques. Diffraction analyses revealed the successful crystallization of pure Li_2SiO_3 single phase by hydrothermal technique, even without further heat-treatments and independent of the surfactant used. Electron microscopy analyses revealed that Li_2SiO_3 powders were composed of uniform micrometric particles with a hollow sphere morphology and nanostructured walls. Finally, different thermal analyses showed that Li_2SiO_3 samples preserved their structure and microstructure after further thermal treatments. Specific aspects regarding the formation mechanism of the spherical aggregates under hydrothermal conditions are discussed, and there is a special emphasis on the effect of the synthesis pathway on the morphological characteristics.

1. Introduction

Lithium ceramics have received considerable attention because of their potential application in the design of breeder ceramics in the nuclear industry [1–4] as ionic conductors in the fabrication of solid electrolytes and anode electrode material for Li-ion batteries [5–7]. Other technological applications also exist, such as the fabrication of gas sensors [8,9] and dry sorbents for CO_2 capture at elevated temperatures [10–13]. Among these ceramics, lithium metasilicate (Li_2SiO_3) has been the subject of several studies [14–19]. Additionally, Li_2SiO_3 has been reported as a promising tritium breeder material in fusion reactors [14,15], as an ionic conductor thin film [16,17] and, more recently, as a candidate for luminescent devices [18,19].

Li_2SiO_3 has been commonly synthesized by solid-state reaction, but other chemical routes have been explored, including sol–gel, microemulsion and modified combustion techniques [20–22]. However, as in other ceramic systems, it is difficult to obtain ultrafine particles of lithium-based materials by conventional methods because the firing of precursor mixtures at elevated temperatures promotes sintering. Currently, there are several emerging synthetic approaches to design and obtain useful advanced ceramics at relatively low temperatures [23–25]. Chemical synthesis provides the possibility to obtain particulate materials with different textural and morphological characteristics that can be valuable and expand the scope of novel applications. Several reports exist describing the use of surfactants added in different routes of chemical synthesis, which not only affect the crystallization of single particles, but also influence the formation of complex microstructures [26–31], especially in bottom-up methods for the synthesis of nanostructured solids [32,33]. These techniques include coprecipitation, sol–gel and surfactant-assisted solvothermal and hydrothermal approaches, among others.

The aim of this work was to systematically study the synthesis of Li_2SiO_3 by a hydrothermal approach using different surfactants (cationic, non-ionic and anionic) and to establish the effect of the synthetic route on the structural and microstructural characteristics of the resultant Li_2SiO_3 powders.

2. Experimental procedure

2.1. Lithium metasilicate synthesis

Lithium hydroxide ($LiOH \cdot H_2O$ 99%, Aldrich) and tetraethyl orthosilicate (TEOS, $Si\text{-}(OC_2H_5)_4$ 98%, Aldrich) were selected as

* Corresponding author. Fax: +52 55 5616 1371.
E-mail address: pfeiffer@iim.unam.mx (H. Pfeiffer).

0022-4596/$ - see front matter © 2011 Elsevier Inc. All rights reserved.
doi:10.1016/j.jssc.2011.03.056

starting materials. Three reagents were used as surfactants: cetyl trimethyl-ammonium bromide (CTAB 99%, Aldrich), octylphenol ethylene oxide condensate (TRITON X-114 99%, Aldrich) or sodium dodecyl benzene sulfate (SDBS 80%, Aldrich), which have cationic, non-ionic and anionic characters, respectively. In the first step, a quantity of the selected surfactant (CTAB, TRITON or SDBS) and LiOH were dissolved in an aqueous ethyl alcohol solution with an alcohol:water volume ratio of 30:70. Stoichiometric quantities of TEOS were added dropwise to the solution under vigorous mechanical stirring. The Li:Si molar ratio was 2:1, and the amount of surfactant was estimated to be 25 times the critical micelle concentration value (cmc) at 25 °C, depending on each surfactant. Therefore, the cmc values were 0.96×10^{-3}, 0.205×10^{-3} and 2.1×10^{-3} mol/L for CTAB, TRITON and SDBS, respectively [34–36]. The solutions were subsequently stirred using an ultrasonic bath for 15 min to obtain a homogeneous sonogel. In a further step, sonogels were transferred into a Teflon-lined stainless steel autoclave vessel, filling it to 80% of its total volume. Hydrothermal reactions were performed at 100, 125 or 175 °C for 20 h, under autogenous pressure, following a heating rate of 5 °C/min. Finally, the autoclave vessel was cooled to room temperature, and the filtered products were washed several times with distilled water and dried at 60 °C for 24 h. The specific hydrothermal reaction conditions were selected based on Pourbaix equilibrium diagrams previously constructed. The diagrams for the Li–Si–H_2O system were drawn for different temperatures using FACTSage (Thermochemical Software and Databases) software [37]. For comparison purposes, Li_2SiO_3 was synthesized by solid-state reaction. The sample was prepared by mixing stoichiometric amounts of silicic acid (H_2SiO_3, J.T. Baker) and lithium carbonate (Li_2CO_3, Sigma Aldrich). The mixture was calcined at 1000 °C for 15 h.

The samples were labeled with a number that corresponded to the hydrothermal synthesis temperature, followed by an abbreviation that indicated which surfactant was used. For example, sample 125TRIT corresponded to a sample synthesized at 125 °C using TRITON X-114 as the surfactant. Samples that were thermally treated were labeled with a final C letter, e.g., 125TRITC. In the case of the samples prepared without surfactant, only the temperature was listed on the label.

2.2. Structural and microstructural characterization

The structural and microstructural characterizations of the different Li_2SiO_3 powder samples were carried out using several techniques. X-ray diffraction (XRD) analysis was performed using a Bruker D8 Advance diffractometer. The crystallite sizes of the synthesized powders were determined from peak broadening using Sherrer's equation: $Dc=(0.9\lambda)/(B\cos\theta)$, where Dc is the crystallite size (nm), λ is the wavelength of the Cu$K\alpha_1$ radiation, θ is Bragg's angle and B is the instrumental corrected full width at half medium. The instrumental contribution for line broadening was subtracted before estimating the crystallite size, assuming that peak shapes were Gaussian and the relation used was as follows: $B^2=B^2_{exp}-B^2_{inst}$, where B_{exp} is the experimentally measured FWHM and B_{inst} is the FWHM due to the instrument. Lithium metasilicate has an orthorhombic crystal system, XRD data were processed using the WinPLOTR software to precisely measure the lattice parameters [38], subsequently, Cohen's analytical method was used [39].

Microstructural and morphological analyses were performed using scanning and transmission electron microscopy techniques. Scanning electron microscopy (SEM) samples were sputter-coated with gold prior to examination. The analysis was performed using a Philips-XL30ESEM electron microscope. For transmission electron microscopy (TEM), a JEOL model JEM-1200EX microscope was used, operating at 120 kV. In addition, a high resolution TEM (HRTEM) technique was performed using a FEI-Tecnai model F-20 transmission electron microscope, operating at 200 kV. In both cases, samples were prepared by standard gravimetric methods. Finally, samples were evaluated by thermogravimetric analysis (TGA) to determine the presence of residual surfactants. The experiments were performed using a Q500HR thermobalance from TA Instruments at 10 °C min^{-1} from 30 to 700 °C in air.

3. Results and discussion

The Pourbaix equilibrium diagrams for the Li–Si–H_2O system with a total concentration of [0.8] at temperatures of 100 and 175 °C are shown in Fig. 1. The information is displayed as a pH vs. electrochemical potential (Eh) plot, and it can be used to estimate the phases in equilibrium during the hydrothermal processes [40–42]. The Eh–pH diagram at 100 °C (Fig. 1a) reveals that the Li_2SiO_3 phase is stable up to pH values of ~9.2. If the temperature is increased to 175 °C (Fig. 1b), the Eh–pH diagram shows that the stability area corresponding to LiOH (aq)+Li_2SiO_3 becomes greater; this result was also true for the Li^++Li_2SiO_3 species. It is noted that the stability limits of these areas change to lower pH values (~8.2). Therefore, thermodynamic data suggested that Li_2SiO_3 can be synthesized at temperatures as low as 100 °C. However, the reaction was carried out at 125 and 175 °C to study the effect of temperature and the possible kinetic effects during synthesis.

All samples were fitted to the JCPDS file 29-0828. The presence of surfactants did not promote the formation of any other secondary phase. Fig. 2 shows the XRD patterns of the samples synthesized at 100 °C with and without surfactants. In some cases, the temperature during synthesis produced minor changes in the relative intensities of the XRD pattern profiles. Fig. 3 shows the XRD patterns corresponding to the samples prepared using CTAB at different temperatures. It was observed that these diffraction patterns fit with the JCPDS file 29-0828 (Fig. 2a). When the temperature was increased to 125 and 175 °C, the (1 1 1) peak (located at 26.9°) became the most intense, rather than the (0 2 0) plane (19.5°, 2θ). Similar behaviors were observed for Li_2SiO_3 powders obtained by a solid-state reaction [15]. The samples corresponded to a base-centered orthorhombic Li_2SiO_3 phase with space group $Cmc21$ (No. 36), this phenomena was explained in terms of crystal growth and preferential orientations. Interestingly, the samples prepared using TRITON did not show this behavior (data not shown). These samples were consistent with the relative intensities of the JCPDS file 29-0828 for all the different hydrothermal temperatures. Figs. 2 and 3 display the XRD pattern profiles and show some differences in line broadening and relative intensities, which indicated that surfactant addition and processing temperature have effects on the structural and microstructural characteristics of the materials.

In general, SEM micrographs showed the formation of self-assembled spherical superstructures. Special characteristics were observed on each sample as a function of the surfactant. The sample morphology did not vary as a function of temperature. Fig. 4 shows the morphology of all samples obtained at 125 °C and the sample obtained by solid-state reaction. While Li_2SiO_3 powders obtained without surfactant presented particle sizes between 0.8 and 1.5 μm, powders synthesized in the presence of surfactants were larger in size and were estimated between 2 and 3.2 μm. Additionally, samples prepared with surfactant were hollow microspheres that were composed of smaller spheres. As expected, the morphology of the sample prepared by solid-state reaction was significantly different, presenting very dense and large polyhedral particles. Fig. 5 emphasizes the

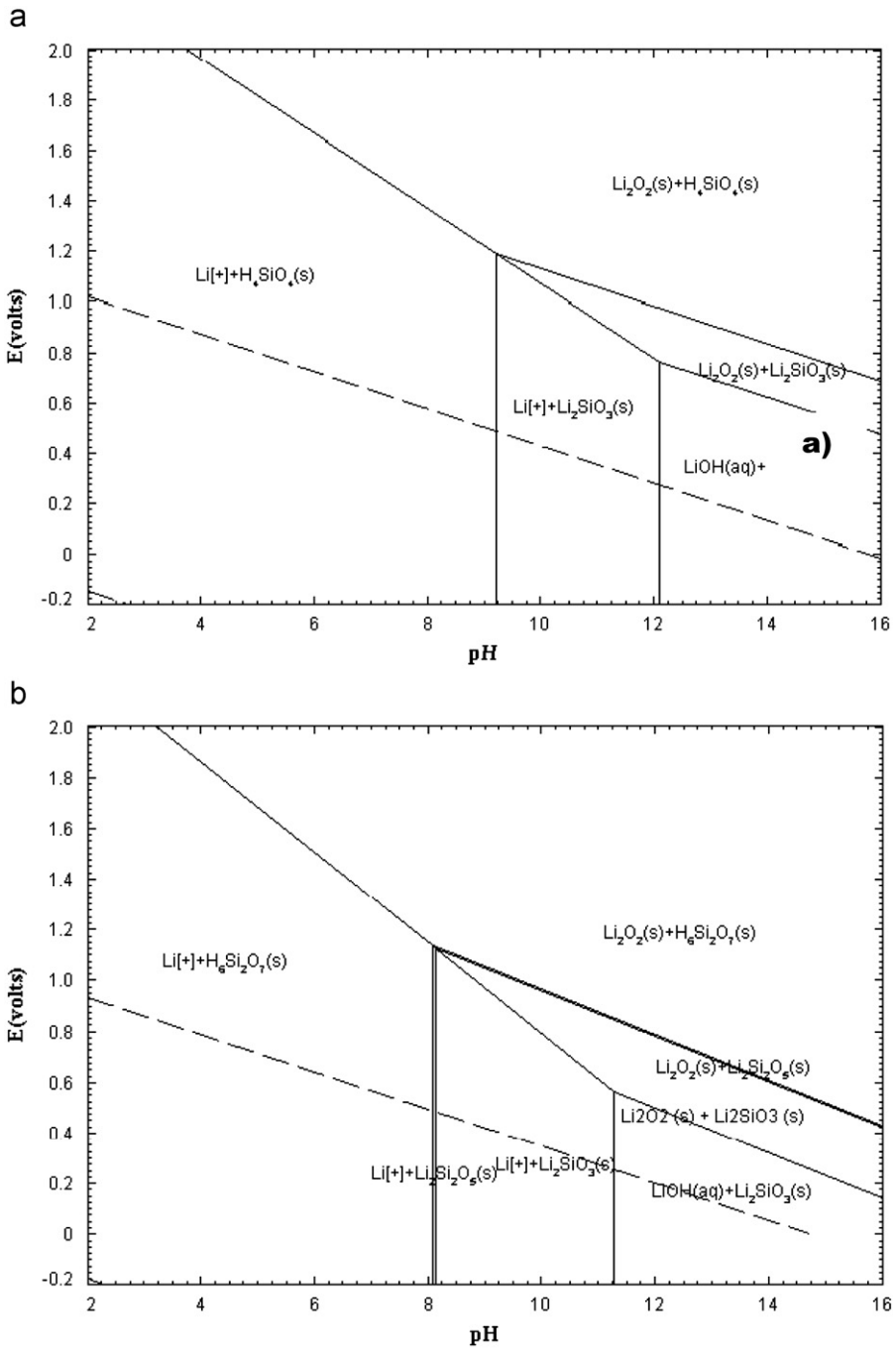

Fig. 1. Eh–pH diagrams of the Li–Si–H_2O system showing predominance species domains. Diagrams were obtained considering a metal's ratio of $0.2 < Si/(Li+Si) < 0.333$, and temperatures equal to: (a) 100 °C and (b) 175 °C.

morphology of one of these samples (100TRIT). It was clearly observed that hollow microspheres were comprised of smaller spheres with particle sizes lower than 400 nm (inset Fig. 5). The presence of those smaller spheres was observed in the samples prepared using TRITON as the surfactant; however, it was not exclusive to those samples, and the powders synthesized with surfactant generally presented similar morphologies.

After microstructural analysis, the thermal stability of the samples was studied by thermogravimetric analysis (Fig. 6). The first weight loss occurred at a temperature below 170 °C (0.85–2.7 wt%), and it was attributed to adsorbed water trapped into the porous and/or interparticle sites. At temperatures above 170 °C, a second weight loss was exhibited, which varied among the samples between 1.18 and 6.54 wt%. This result was attributed to the thermal decomposition of the residual surfactants. All of the organics were decomposed and released before the temperature reached 500 °C. Based on these results, all the samples were thermally treated at 400 °C for 3 h in air to completely eliminate the organic residues.

Fig. 7 presents the XRD pattern and SEM image of the calcined 100TRITC sample. As observed, there were not significant changes either in the spherical morphology or phase, indicating the thermal stability of the samples. Table 1 summarizes the structural and microstructural characteristics of all samples, before and after the thermal treatment. In general, all samples were nano-crystalline materials with $Dc < 30$ nm. However, two

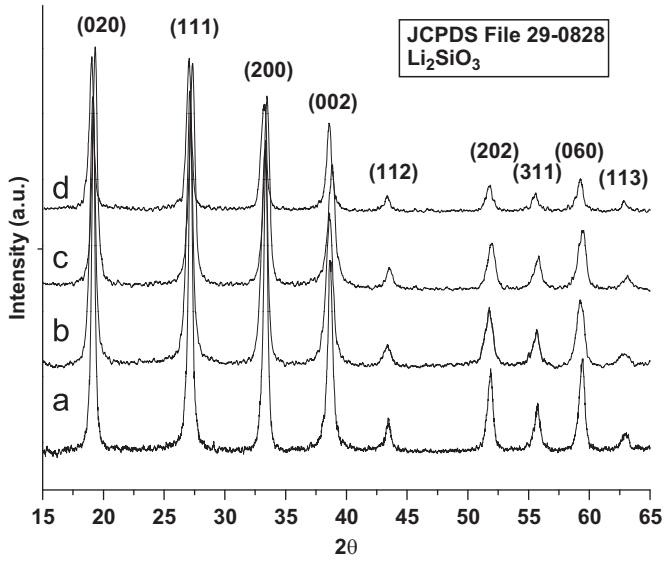

Fig. 2. XRD patterns of as prepared lithium silicate powders. The different samples are: (a) 100, (b) 100CTAB, (c) 100SDBS and (d) 100TRIT.

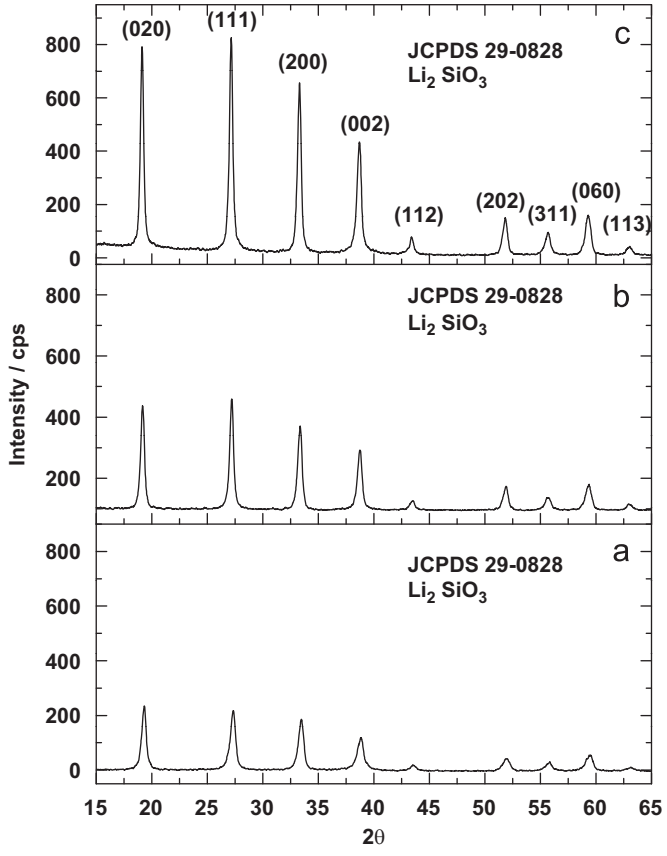

Fig. 3. XRD patterns of as prepared lithium silicate powders, using CTAB as surfactant. The different samples are: (a) 100CTAB, (b) 125CTAB and (c) 175CTAB.

different behaviors were observed. The first behavior showed how crystallite size tends to grow as a function of the hydrothermal temperature, and the second indicated that samples prepared with surfactant show smaller crystallite sizes than samples synthesized without surfactant. The smallest crystallite size, 14 nm, was obtained when the sample was prepared using TRITON X-114 as surfactant and the hydrothermal reaction was conducted at 100 °C. Table 1 contains the cell parameter values as estimated by Cohen's analytical method. These values are consistent with the cell parameter values reported on the JCPDS file 29-0828, which are as follows: $a=5.3975$ Å, $b=9.3974$ Å and $c=4.6615$ Å.

To further analyze the microstructure characteristics of the samples, conventional and high-resolution TEM studies were carried out. Bright field images corresponding to the 175 and 175TRIT samples are shown in Fig. 8. Two different microstructures are observed. It was evidenced that when the surfactants were not used, some concentric or multi-shelled spheres were formed (see arrows on Fig. 8a). This type of microstructure has been reported for systems in which a template is not used and Oswald ripening is the primary promoter for hollow microstructures formation [43–45]. Qiao et al. [46] and Guan et al. [47] identified the microstructure of multi-shelled sphere as an intermediate step during the formation of hollow spheres through Oswald ripening. Alternatively, in the case of surfactant addition, it can be observed that hollow microspheres are composed of smaller spheres with a diameter of approximately 350 and 400 nm (Fig. 8b and c). TEM images showed that the smaller aggregates also presented hollow microstructures (Fig. 8c). Finally, other images reveal that the sphere walls are comprised of nano-particles (Fig. 8d). The same morphological characteristics were observed in the samples synthesized at different temperatures after calcination. Fig. 9 displays a high resolution TEM image of the 100-TRITC sample, and it is evident that the hollow microstructures of the spherical aggregates are built up by nanoparticles smaller than 50 nm. The HRTEM image shows crystalline nanoparticles and different domains of approximately 10–20 nm, which are in good agreement with the results calculated by XRD (see Table 1).

Results from the syntheses are summarized. In the first step of the synthesis, the sol–gel preparation involved an alkoxide (TEOS) and a salt as the precursors ($LiOH \cdot H_2O$). In this case, $LiOH \cdot H_2O$ was dissolved in an aqueous-alcoholic solution, and TEOS was added dropwise. Therefore, water must be used for the TEOS hydrolysis, which occurs as follows:

$$Si(OC_2H_5)_4 + nH_2O \rightarrow Si(OH)_n(OC_2H_5)_{4-n} + nC_2H_5OH \quad (1)$$

If lithium reacts with partially hydrolyzed silica, soluble metallosiloxanes must be formed; for example, if $n=2$:

$$Si(OH)_2(OC_2H_5)_2 + 2C_2H_5OH + 2LiOH \rightarrow (OC_2H_5)_2Si^{-O-Li}_{-O-Li} + 2C_2H_5OH + 2H_2O \quad (2)$$

The hydrolysis reaction is dependent on the basic pH of the solution, and the condensation should be promoted by the surfactant concentration. The conversion from the intermediate state to a metal oxide is finally dependent on the hydrothermal conditions. Because polymeric units are hydrolyzed at elevated temperatures and pressures during a hydrothermal reaction, different oligomers can be formed as a result of ionization and polymerization reactions. After Li_2SiO_3 spontaneous hydrothermal nucleation, re-dissolution and re-crystallization of the already-formed primary particles could have occurred. In this second step, Oswald ripening phenomena must take place. However, when the system involves the use of a surface active agent, the interaction between the particle surfaces and the surfactants occurs as soon as the primary particles of Li_2SiO_3 are formed and have acquired the characteristics of a metal oxide surface. Surfactant molecules are adsorbed through electrostatic interactions, inhibiting further re-dissolution and re-crystallization processes. Hence, the adsorbed species on the ceramic surface hinder the coalescence of primary particles and further growth. These factors can explain the small crystallite size obtained when

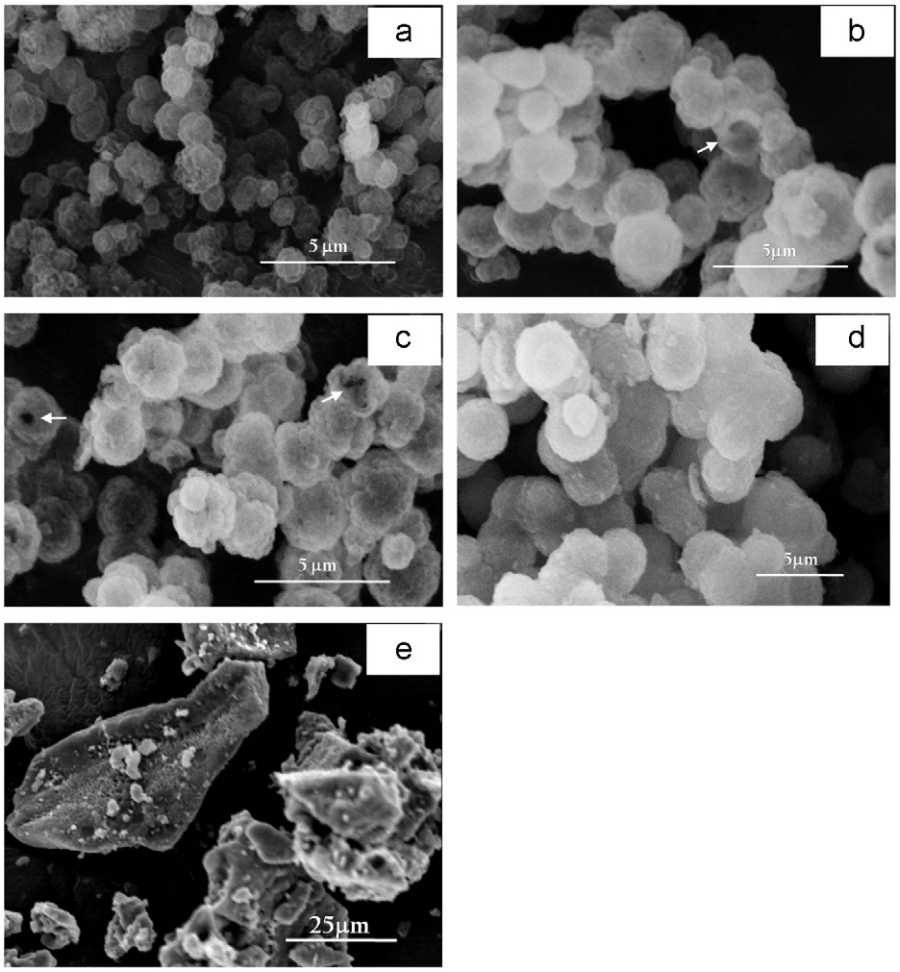

Fig. 4. SEM images of samples prepared by solid state reaction and by hydrothermal synthesis in the presence of different surfactants. The different samples are: (a) 125, (b) 125CTAB, (c) 125TRIT, (d) 125SDBS and (e) solid state reaction.

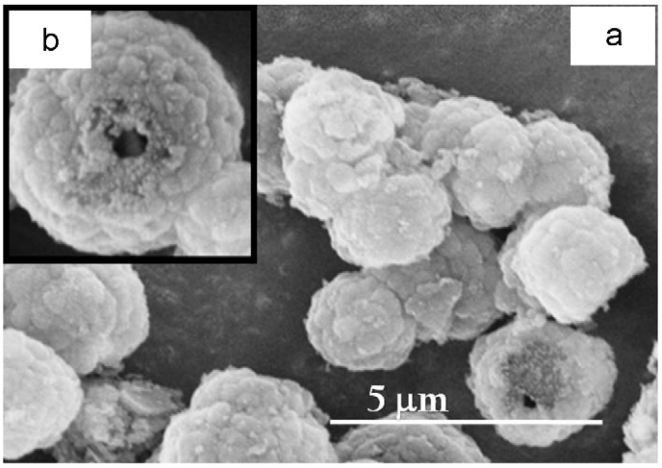

Fig. 5. SEM image of the sample 100TRIT. The inset shows an image of one spherical particle, which was built up by smaller ones.

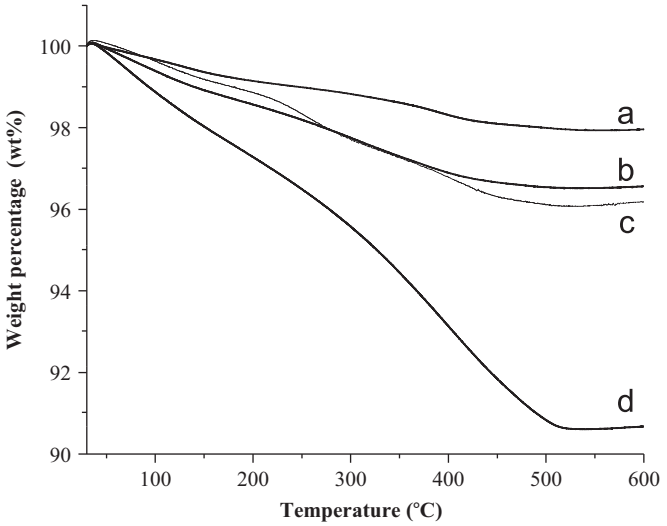

Fig. 6. TGA curves of Li_2SiO_3 powders under an atmosphere of air: (a) 100, (b) 100CTAB, (c) 100SDBS and (d) 100TRIT.

surfactant is used (Table 1). Additionally, the formation of double-hollow microstructures could occur as follows:

(1) *Li_2SiO_3 primary nanoparticle self-essembly*: In a first step, primary Li_2SiO_3 particles are formed. Due to electrostatic interactions, these particles are adsorbed onto the surface of the previously formed supramolecular assemblies of the surfactant; the assemblies play the role of templates. Some authors have reported the formation of spherical micelle arrays of surfactant in aqueous solutions, which act as a soft template and promote the formation of hollow microstructures [48,49]. In the present work, because the hollow

smallest diameter spheres are considerably larger than the size of a single micelle, other supramolecular assemblies, such as vesicles, could be acting as a soft template.

(2) *Aggregation of the smallest spheres into the formation of hollow microspheres*: Considering ethanol produces gas bubbles, the evolution of the bubbles could promote particle aggregation once the primary spherical aggregates are formed. As in the surfactant micelles case, this phenomenon may also explain the formation of hollow microstructures in different materials prepared by hydrothermal processing [50–52]. Different gas microbubbles may be considered as aggregation centers or temporary soft templates. Here, it is suggested that assembles of such particles are formed as a result of the interaction between the hydrophobic tiles of surfactant molecules, which are adsorbed onto the surface of spherical primary aggregates, and the gas–liquid interface.

(3) *Oswald ripening*: Oswald ripening has been proposed as a synthetic approach for the preparation of hollow particles [52]. Briefly, this phenomenon is defined by the IUPAC as the growth of larger crystals from smaller ones. During the hydrothermal process, high temperatures and long reaction times favor the Oswald ripening phenomenon. The morphology of both small and large spheres must keep changing, meaning that Oswald ripening may lead to the evacuation of the central space in the spherical aggregates through crystallite growth, producing hollow microstructures. The proposed growth mechanism of the double-hollow microstructure formation is supported by both SEM and TEM results.

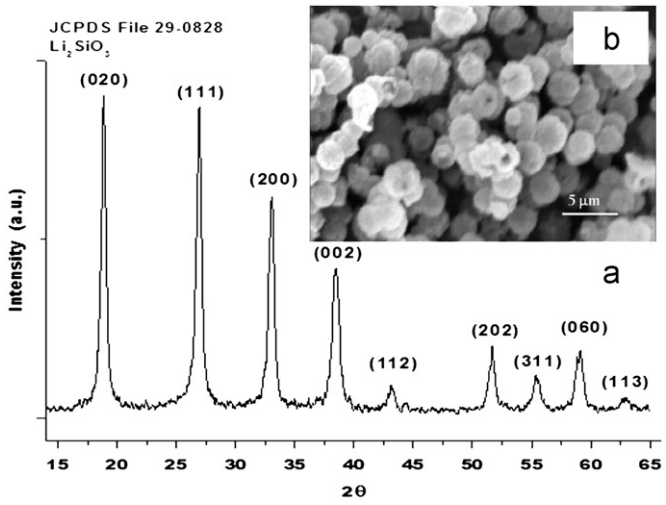

Fig. 7. XRD pattern and SEM image (inset b) of the sample 100TRITC after calcination at 400 °C for 3 h in air.

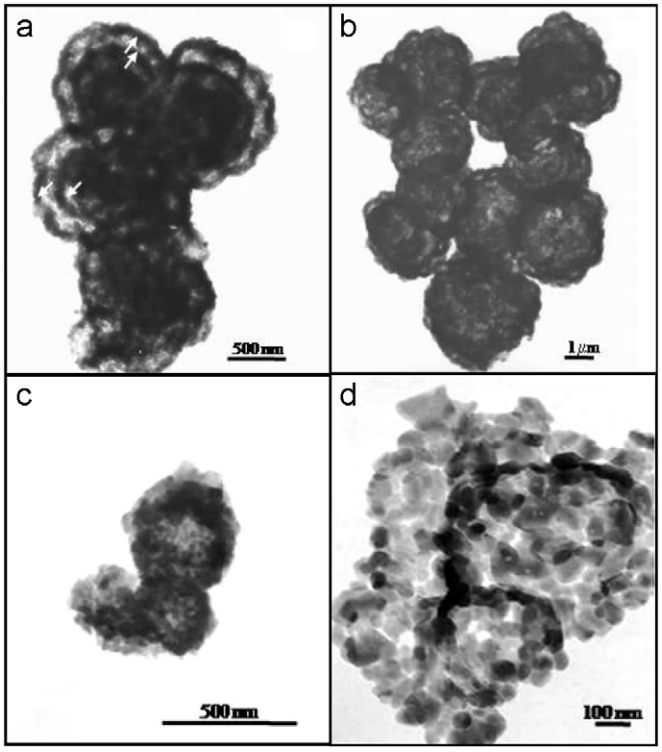

Fig. 8. Bright field TEM images of the samples 175 (a) and 175TRIT from (b) to (d).

Table 1
Crystallite size and cell parameters of the prepared samples.

Sample	Temperature of hydrothermal crystallization (°C)	Cell parameters (Å)			Crystallite size (nm)[a]	
		a	*b*	*C*	Without further thermal treatment	After calcination at 400 °C
Solid state	1000[b]	5.403	9.358	4.667	—	—
Without	100	5.402	9.353	4.670	24	28
	125	5.409	9.369	4.667	26	29
	175	5.409	9.371	4.676	27	32
CTAB	100	5.416	9.379	4.680	16	18
	125	5.410	9.374	4.678	22	24
	175	5.405	9.365	4.669	26	28
SDBS	100	5.415	9.381	4.683	17	19
	125	5.410	9.371	4.678	18	21
	175	5.410	9.369	4.674	27	30
TRITON X-114	100	5.414	9.377	4.684	14	17
	125	5.410	9.374	4.677	22	24
	175	5.409	9.371	4.676	28	29

[a] Crystallite size for the [1 1 1] plane.
[b] Calcination at 1000 °C for 15 h.

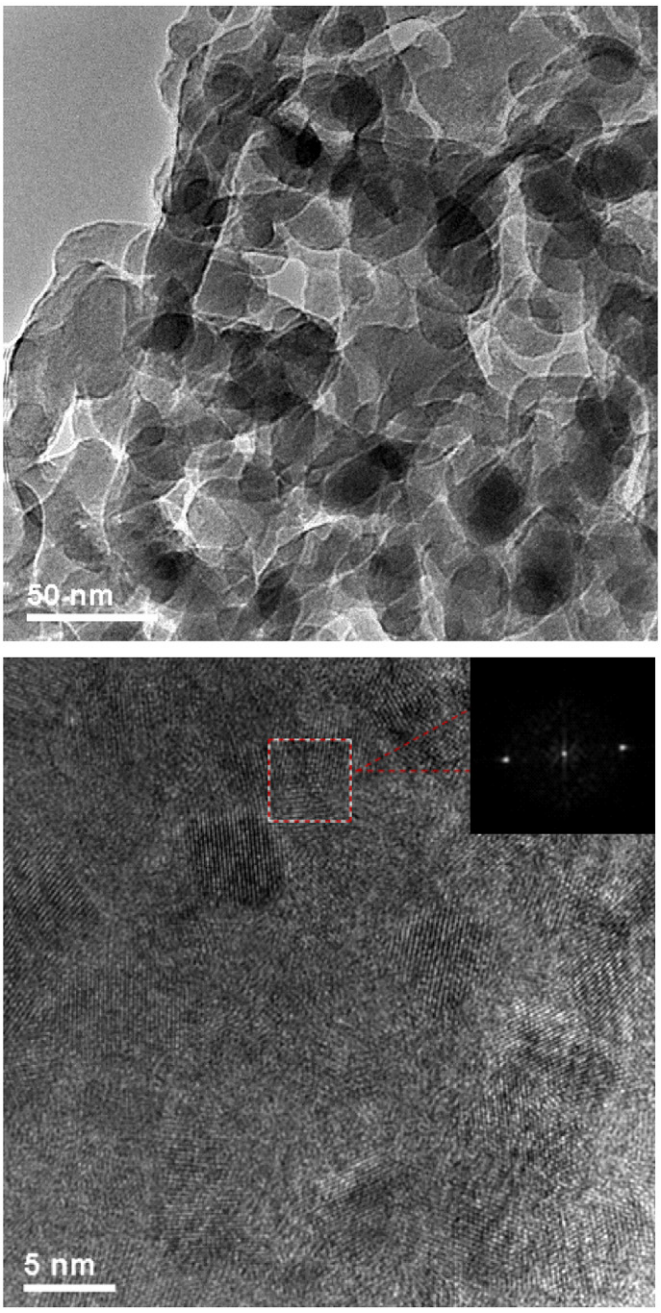

Fig. 9. Bright field TEM images of sample 100TRITC showing the nanostructured walls and HRTEM image showing the nano-crystalline domains.

4. Conclusions

Different nano-crystalline Li_2SiO_3 samples were successfully synthesized using a hydrothermal method in the absence and presence of various surfactants (TRITON X-144, CTAB and SDBS). Initially, XRD results showed that although the syntheses produced Li_2SiO_3, the presence of the surfactants and the temperature of synthesis modified the structural and microstructural characteristics of the materials. Scanning electron microscopy characterization revealed the formation of nanostructured and hollow spherical aggregates. The results were corroborated by TEM, where two different microstructures could be observed. If surfactants were not used, some concentric or multi-shelled spheres were formed; this result was explained by the Oswald ripening phenomenon. When surfactants were used, the hollow microspheres were composed of smaller spherical aggregates, which also presented hollow microstructures.

In light of these results, a formation mechanism for spherical aggregates was proposed based on the surfactant addition effect and hydrothermal treatment temperature. It is believed that both factors played crucial roles in controlling the morphology and microstructure properties. Finally, these materials are stable and preserved their morphological characteristics after calcinations at 400 °C.

Acknowledgments

This work was financially supported by ICyT-DF (179/2009) and PAPIIT-UNAM (IN100609). J. Ortiz-Landeros thanks CONACYT and PIFI-IPN (project SIP-20100073). Authors thank Carlos Flores for the technical help.

References

[1] N. Roux, S. Tanaka, C. Johnson, R. Verrall, Fusion Eng. Design 41 (1998) 31.
[2] D. Cruz, S. Bulbulian, J. Nucl. Mater. 312 (2003) 262.
[3] R. Knitter, B. Alm, G. Roth, J. Nucl. Mater. 367–370 (2007) 1387.
[4] H. Pfeiffer, P. Bosch, S. Bulbulian, J. Nucl. Mater. 257 (1998) 309.
[5] Y. Tomita, H. Matsushita, H. Yonekura, Y. Yamauchi, K. Yamada, K. Kobayashi, Solid State Ionics 174 (2004) 35.
[6] Y. Abe, E. Matsui, M. Senna, J. Phys. Chem. Solids 68 (2007) 681.
[7] D.R. Zhang, H.L. Liu, R.H. Jin, N.Z. Zhang, Y.X. Liu, Y.S. Kang, J. Ind. Eng. Chem. 13 (2007) 92.
[8] J.W. Fergus, Sensor. Actuat. B 134 (2008) 1034.
[9] N. Imanaka, Y. Hirota, G.Y. Adachi, Sensor. Actuat. B 242 (1995) 380.
[10] B.N. Nair, R.P. Burwood, B.J. Goh, K. Nakagawa, T. Yamaguchi, Prog. Mater. Sci. 54 (2009) 511.
[11] J. Ida, R. Xiong, Y.S. Lin, Sep. Purif. Technol. 36 (2004) 41.
[12] J.D. Figueroa, T. Fout, S. Plasynski, H. Mcllvried, R.D. Srivastava Inter., J. Greenhouse Gas Control 2 (2008) 9.
[13] H. Pfeiffer, Advances in CO_2 Conversion and Utilization; Advances on Alkaline Ceramics as Possible CO_2 Captors, Chapter 15, ACS, 2010.
[14] D. Cruz, S. Bulbulian, E. Lima, H. Pfeiffer, J. Solid State Chem. 179 (2006) 909.
[15] T. Tang, Z. Zhang, J.B. Meng, D.L. Luo, Fusion Eng. Design 84 (2009) 2124.
[16] S.I. Furusawa, A. Kamiyama, T. Tsurui, Solid State Ionics 179 (2008) 536.
[17] S.I. Furusawa, T. Kasahara, A. Kamiyama, Solid State Ionics 180 (2009) 649.
[18] Y.P. Naik, M. Mohapatra, N.D. Dahale, T.K. Seshagiri, V. Natarajan, S.V. Godbole, J. Lumines. 129 (2009) 1225.
[19] S. Morimoto, S. Khonthon, Y. Ohishi, J. Non-Cryst. Solids 354 (2008) 3343.
[20] B. Zhang, M. Nieuwouldt, A.J. Easteal, J. Am. Ceram. Soc. 91 (2008) 1927.
[21] R.B. Khomane, B.K. Sharma, S. Saha, B.D. Kulkarni, Chem. Eng. Sci. 61 (2006) 3414.
[22] G. Mondragón-Gutiérrez, D. Cruz, H. Pfeiffer, S. Bulbulian, Res. Lett. Mater. Sci. 2 (2008) 1.
[23] C. Bluthardt, C. Fink, K. Flick, A. Hagemeyer, M. Schichter, A. Volpe Jr., Catal. Today 137 (2008) 132.
[24] R. Roy, J. Solid State Chem. 111 (1994) 11.
[25] K. Byrappa, T. Adschiri, Prog. Cryst. Growth Char. Mater. 53 (2007) 117.
[26] Y. Wang, A. Zhou, Z. Yang, Mater. Lett. 62 (2008) 1930.
[27] Z. Tang, L. Hu, Z. Zhang, J. Li, S. Luo, Mater. Lett. 61 (2007) 570.
[28] S. Liu, O.I. Lebedev, M. Mertens, V. Meynen, P. Cool, G. van-Tendeloo, E.F. Vansant, Micropor. Mesopor. Mater. 116 (2008) 141.
[29] F. Khan, M. Eswaramoorthy, C.N.R. Rao, Solid State Sci. 9 (2007) 27.
[30] N.A. Turta, P. De Luca, N. Bilba, J.B. Nagy, A. Nastro, Micropor. Mesopor. Mater. 112 (2008) 425.
[31] S. Wang, H. Xiu, L. Qian, X. Jia, J. Wang, Y. Liu, W. Tang, J. Solid State Chem. 182 (2009) 1088.
[32] J.N. Lalena, D.A. Cleary, E. Carpenter, N.F. Dean, Inorganic Materials Synthesis and Fabrication, John Wiley & Sons Inc., New Jersey, USA, 2008.
[33] C. Yan, L. Zou, D. Xue, J. Xu, M. Liu, J. Mater. Sci. 43 (2008) 2263.
[34] T. Gu, P.A. Galera-Gómez, Colloid. Surf. A: Physicochem. Eng. Aspects 104 (1995) 307.
[35] C. Vautier-Giongo, H.O. Pastore, J. Colloid Interface Sci. 299 (2006) 874.
[36] A.H. Saiyad, S.G.T. Bath, A.K. Rakshit, Colloid Polym. Sci. 276 (1998) 913.
[37] FACTSage Thermochemical Software and Databases. 〈www.factsage.com〉.
[38] WinPLOTR Software. 〈www.cdifx.univ-rennes1.fr/winplotr/winplotr.htm〉.
[39] B.D. Cullity, S.R. Stock, Elements of X-Ray Diffraction, Prentice Hall Inc., Upper Saddle River, New Jersey, 2001.
[40] R. Piticescu, C. Monty, D. Millers, Sensor. Actuator. B 109 (2005) 102.
[41] Y. Tao, Z. Chen, B. Zhu, Physica B 362 (2005) 76.
[42] A. Dias, J. Sol. Chem. 38 (2009) 843.
[43] J. Li, H.C. Zeng, J. Am. Chem. Soc. 129 (2007) 15839.
[44] H.G. Yang, H.C. Zeng, J. Phys. Chem. B 108 (2004) 3492.

[45] Y. Ma, L. Qi, J. Colloid Interface Sci. 335 (2009) 1.
[46] R. Qiao, X.L. Zhang, R. Qiu, J.C. Kim, Y.S. Kang, Chem. Mater. 19 (2007) 6485.
[47] M. Guan, F. Tao, J. Sun, Z. Xu, Langmuir 24 (2008) 8280.
[48] Q. Liu, X. Guo, Y. Li, W. Shen, Langmuir 25 (2009) 6425.
[49] C. Jiang, Y. Wang, Mater. Chem. Phys. 113 (2009) 531.
[50] Y.J. Kim, S.Y. Chai, W.I. Lee, Langmuir 23 (2007) 9567.
[51] S.K. Panda, S. Chaudhuri, J. Colloid Interface Sci. 313 (2007) 338.
[52] H.C. Zeng, Curr. Nanosci. 3 (2007) 177.